Interpretation of Flow Fields Induced by Water Spray Systems in Reduced-Scale Tunnel Fire Experiments by means of CFD Simulations

Jiayun Sun [a,b], Zheng Fang[a,c,*], Tarek Beji[b] and Bart Merci[b]

[a] School of Civil Engineering, Wuhan University, Wuhan, Hubei,430072, China

[b] Department of Flow, Heat and Combustion Mechanics, Ghent University-UGent, B-9000 Ghent, Belgium

[c] Engineering Research CenterofUrbanDisastersPreventionandFireRescueTechnologyofHubeiProvince, 430072, China

* Corresponding author：Zheng Fang

Email address:zfang@whu.edu.cn

Interpretation of Flow Fields Induced by Water Spray Systems in Reduced-Scale Tunnel Fire Experiments by means of CFD Simulations

Abstract

Computational Fluid Dynamics (CFD) simulation results, obtained with FDS 6.0.1 (McGrattan et al., 2013), are presented of reduced-scale tunnel fire tests. In (Sun et al., 2016), an extensive data set has been discussed in terms of temperature measurements in a reduced-scale tunnel, involving longitudinal ventilation and a variety of water supply through nozzles, in the context of potential smoke blockage. In (Sun et al., 2016), 10 different scenarios have been discussed, for different numbers of nozzles and different nozzle configurations. Given the limitation of the experimental instrumentation, as a series of thermocouple trees, a full interpretation of the flow field was impossible. Nevertheless, a detailed characterization and interpretation of this turbulent flow field under different circumstances is essential in the discussion of potential smoke blockage. To that purpose, CFD can be a very useful tool. In this paper, as a first step, results are presented for 2 cases, without mechanical longitudinal ventilation, in order to illustrate the validity and potential of the CFD simulations, with and without the water system (4 nozzles) activated. The validity of the CFD results, using the default FDS settings for turbulence and combustion modeling, is illustrated first through comparison of the temperature profiles with the experimental data. A comprehensive sensitivity study on the computational mesh and model settings for the water sprays is included. Subsequently, the mean flow and temperature fields are analyzed, providing significant additional insight into the impact of the water system. The entrainment, induced by the water sprays, is illustrated. This causes downward motion of the smoke in the sprays. By bumping onto each other, the impinging flows onto the floor in their turn create an upward flow in between the water spray envelopes that impinges onto the ceiling in the absence of longitudinal ventilation. The global effect is smoke blockage by the water system.

Keywords*: CFD simulations, FDS, tunnel fire, water system*

1 Introduction

In(Sun et al., 2016), a series of experiments has been discussed, illustrating the effect of mechanical longitudinal ventilation and water sprays on fire-induced smoke motion in a reduced-scale tunnel. The context of those experiments was to test the effectiveness of water systems in blocking the fire-induced smoke and heat, under different ventilation and water spray conditions. To that purpose, a water system consisting of several water nozzles was put in place. Different combinations of numbers of nozzles, water flow rates and positions of nozzles were discussed in (Sun et al., 2016)..

The detailed information of the experimental setup was provided in(Sun et al., 2016).Some of important aspects are briefly repeated here. The tunnel was made of fire-proof glass and iron plate, with thermo-physical properties as presented in section 2. The temperatures have been measured with unshielded K-type thermocouples, with accuracy of ±0.1℃. A weighting platform, with ±0.1g accuracy, was placed underneath the fuel pan to measure the fuel mass loss rate. Although, the amount of instrumentation in (Sun et al., 2016) was limited, essentially measuring temperatures by means of thermocouple trees, spread over the tunnel. This is a very typical situation in fire experiments, i.e., only a limited amount of experimental data can be collected and in particular flow field measurements are hard, if not impossible, to do. So it is necessary for using numerical approaches to have an insight into the flow field induced by the water sprays, particularly for the gas entrainment phenomena(Morgan and Baines, 1979; Sirignano, 1999; St-georges and Buchlin, 1994).

There are a number of numerical models to simulate the interaction of fire smoke and water spray. One-dimensional models (Chow and Yao, 2001; Cooper, 1995; Li and Chow, 2008; Tang et al., 2014; Tang et al., 2013)are simple and have short calculation times. However, these models rely upon many assumptions on flow motion and gas properties, and calculating the detailed flow field is not possible. Considering the complex phenomena observed in (Sun et al., 2016), CFD is a potentially useful tool to interpret the experimental data and CFD packages have been widely used to simulate fire smoke motion and water sprays to obtain detailed flow

fields (Blanchard et al., 2014; Deckers et al., 2013; Hua et al., 2002; Kim and Ryou, 2003; Merci and Van Maele, 2008; Van Maele and Merci, 2008).

Therefore, it can be interesting to supplement the experimental data with CFD results, so that more information on the flow (and temperature) field is obtained(Merci, 2014). This allows to improve our understanding of the interaction between water sprays and the fire-induced smoke motion, potentially combined with the effect of longitudinal mechanical ventilation.

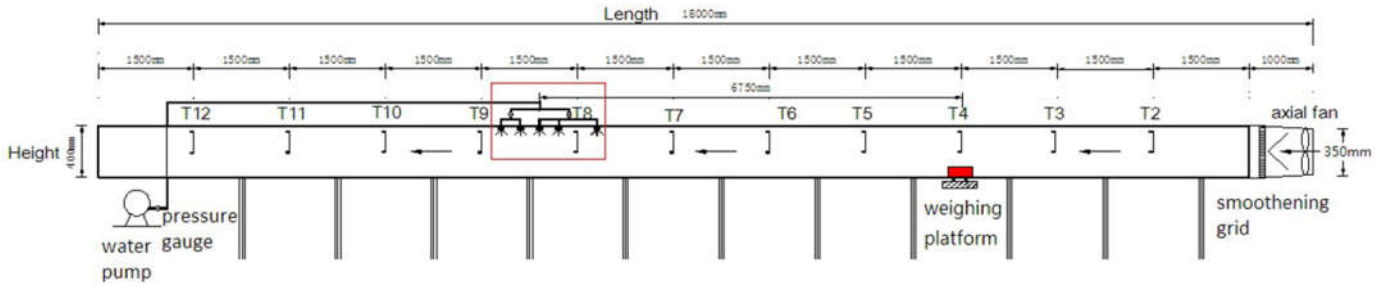

Figure 1. Sketch of the reduced-scale tunnel (side view: vertical section in the mid-plane). T2 – T12 refer to thermocouple trees.

For obvious reasons, the quality of the CFD results must be assessed first. This is a first objective of the present study, comparing temperatures obtained with FDS to experimental data. Unfortunately, a full direct one-to-one comparison is not possible, because a few aspects were not measured in (Sun et al., 2016): the possible effect of wind (which could have some impact, particularly on the tests without longitudinal ventilation), the effect of leakage (some smoke leakage was observed in the experiments of (Sun et al., 2016), but this was not quantified) and the detail of the inlet fan for cases with mechanical ventilation. Nevertheless, the study of the flow field by itself remains possible, as long as the CFD simulations are of high quality. To that purpose, an extensive sensitivity study is performed on the computational mesh, as well as on the settings for the water sprays, to verify that the CFD results are not very sensitive on these aspects.

Subsequently, the flow and temperature fields as obtained with FDS, are discussed in detail. In this paper, only 2 the experiments of (Sun et al., 2016) are simulated as first step of the over-all study, namely 2 cases without

longitudinal ventilation (i.e., there is only natural ventilation), once with the water system activated and once without (see Table 1).These are Tests 1 and 3 from (Sun et al., 2016) (2 × 2 nozzles, with water flow rate equal to 1.94l/min per nozzle). The in-depth discussion of flow and temperature fields is the second important objective of this study.

It is recalled that in (Sun et al., 2016), other water flow rates and other nozzle configurations were also considered, but a CFD study for those cases is considered as future work and the present paper serves as a first step in the over-all study.

Simulation No.	Longitudinal ventilation	Water System
1	NO	NO
3	NO	YES

Table 1. Overview of the configurations. The water system consists of 2 x 2 nozzles, with flow rates of 1.94l/min per nozzle. The numbering of simulations corresponds to the numbering of the tests in (Sun et al., 2016).

2 Simulation set-up and sensitivity study

A detailed description of the configuration is provided in(Sun et al., 2016).Therefore, only the details required for the numerical simulations are repeated here. The tunnel (18m long × 1.1m wide × 0.4m high) is made of fire proof glass(8 mm thick, ρ= 2700 kg/m^3 , c = 0.84 kJ/kg·K and k = 0.76W/m·K(Drysdale, 2011)). Above the fire source, an iron plate replaced the glass over an area of 1m × 1.5 m(thermal properties of the iron plate: density: ρ =7850kg/m^3,c = 0.46 kJ/kg·K and k = 45.8W/m·K(Drysdale, 2011)).Ambient temperature is set to 20 ^{o}C.

The default FDS 6 model settings are applied for turbulence, combustion and radiation, with a radiative fraction set to 0.16 (Drysdale, 2011).

The fuel is methanol, contained in an iron tray (25cm × 20cm×5cm) positioned on the floor at the center of the cross section and4.5m away from the entrance of the tunnel. The initial fuel height in the experiments is 3 cm. In the simulations, the prescribed height allows to have a gas phase mesh well aligned with the initial fuel surface

when cell sizes of 1 and 1.5 cm are used; it is set to 4 cm when the cell size is 2 cm. Figure 2 reveals the imposed (and experimentally determined) heat release rate as function of time. First, there is a linear increase from 0 to 10.7kWwithin 10s. Subsequently, there is an additional linear increase (until t = 100s) to the steady state value (16kW).

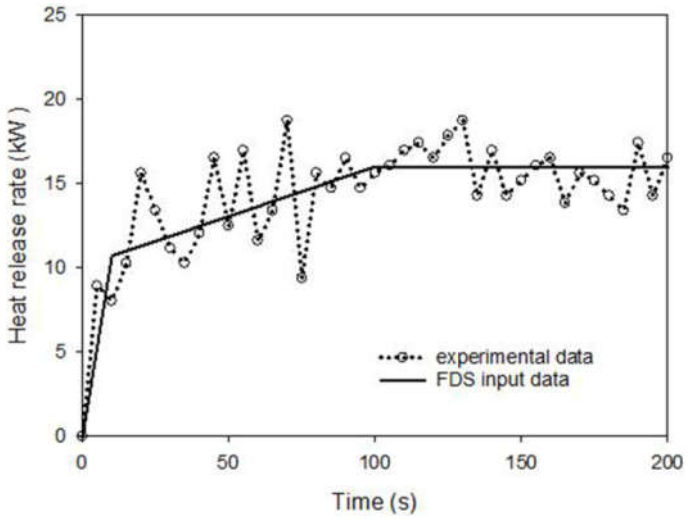

Figure 2. Temporal evolution of experimentally measured and imposed heat release rate.

In inlet and outlet boundary conditions are prescribed as 'OPEN'. The computational domain has been extended over a distance of 0.54 m in order to reduce the impact of the boundary conditions (see Fig. 3).

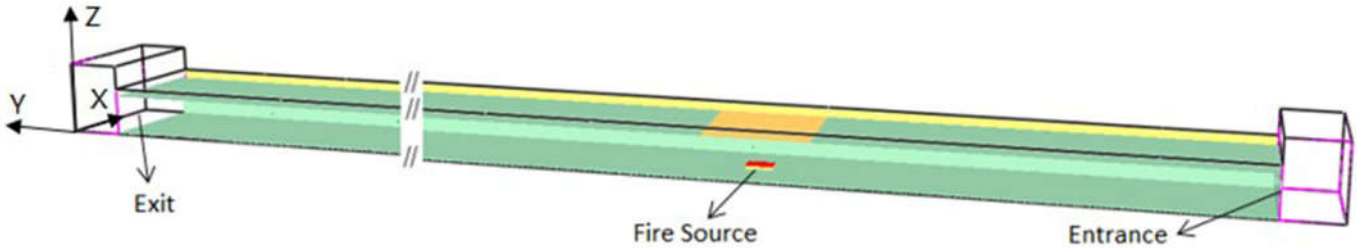

Figure 3. Sketch of the computational domain (from Smokeview).

In the experiments, the water system was activated 20s after ignition with 0.5 MPa working pressure, creating 74^{o} full cone water sprays through each nozzle(Sun et al., 2016). In the simulations, the corresponding water flow rate (1.94 l/min per nozzle) is imposed. The distribution of the water droplets size is discussed in detail below.

As in the experiments,20 thermocouples are defined in the mid-plane, recording temperatures every 5s. Table 2 provides the positions of the thermocouples, discussed in the present paper. Additionally, in order to study the flow and temperature fields, 4slicesare defined: 2 vertical slices(one in the mid-plane, x=0.56m, and one underneath 2 nozzle heads, x=0.26m), and 2 horizontal slices at different height (at mid-height, z=0.2m, and at thermocouple height just below the ceiling, z=0.36m).

Label	5-1	5-2	7-1	7-2	10-1	10-2	11-1	11-2
y (m)	6	6	9	9	13.5	13.5	15	15
z (m)	0.36	0.2	0.36	0.2	0.36	0.2	0.36	0.2

Table 2. Labels and positions (in m) of the thermocouples discussed in the present paper.

2.1 Sensitivity studies

2.1.1 Grid sensitivity study

In(McGrattan et al., 1998),the D* criterion is reported in the context of LES simulations of fire plumes. It is stated that the mesh size should be smaller than D*/10, with D* the characteristic length scale of the fire:

$$D^* = \left(\frac{\dot{Q}}{\rho_\infty T_\infty c_P \sqrt{g}} \right)^{2/5}$$

For $\dot{Q} = 15.2kW$and$\dot{Q} = 16kW$, the value of D^* is approximately0.18m. This implies that a mesh size of 1.8 cm or less should provide reliable results.

However, this is not the only criterion here, because there is a tunnel configuration with fire-induced horizontal flow. This implies that a sufficient number of grid cells is required over the tunnel height (Tilley et al., 2011; Van Maele and Merci, 2008). In the configuration at hand, where the tunnel height (0.4 m) is more than twice the value of D^*, the D^* criterion is the most stringent. Also the smoke layer (see below) in the cases with stratification is sufficiently resolved with mesh sizes of 1.8 cm or less for the case at hand.

Nevertheless, a mesh size sensitivity study is carried out here, with three different grid sizes: 2cm × 2cm × 2cm, 1.5cm × 1.5cm × 1.5cm and 1cm × 1cm × 1cm, for scenario 1 (Table 1).

Figure 4provides the temperature profiles across the tunnel at mid-height (z=0.2m) and near the ceiling (z=0.36m) as obtained on the different meshes. Average values are presented, obtained from 100s to 200 s, which is a period with steady heat release rate. Relatively strong differences are observed for the 2cm × 2cm×2cm mesh at mid-height. The reason is that the smoke layer (visualized by means of temperature contours in Fig. 5) is slightly thicker on this mesh, so that the temperature rise is just felt at mid-height on this mesh, while it is not felt on the finer meshes. It must be noted that, as mentioned, the fire source is also positioned 1 cm higher (at 4 cm height, rather than 3 cm height) compared to the other meshes, which may partially explain differences in results obtained on this mesh. Near the ceiling, all deviations are below 10%. Based on these observations, the decision has been made to use the 1.5cm × 1.5cm × 1.5cm mesh for the CFD calculations in the present study.

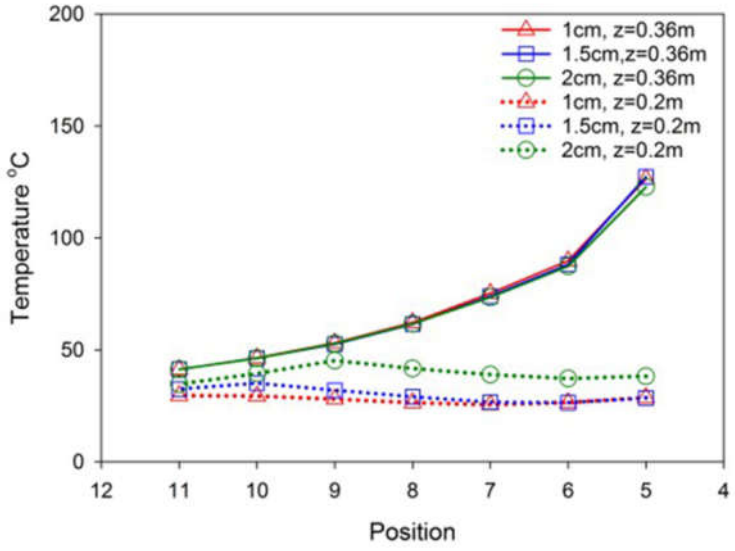

Figure4. Grid sensitivity: comparison of temperatures for 3 mesh cell sizes for Simulation1. Positions: see Table 2. Values have been averaged over the period 100s – 200s (steady heat release rate).

Additionally, Figure 5 shows temperature contour plots in the vertical mid-plane. As mentioned, the smoke layer is thicker on the coarser mesh, which results in higher temperatures at mid-height (z=0.2m), while almost the

same smoke layer thickness is obtained on the 1.5cm and 1cm grids. This confirms the choice of using the 1.5 cm × 1.5 cm × 1.5 cm mesh for the CFD calculations in the present study.

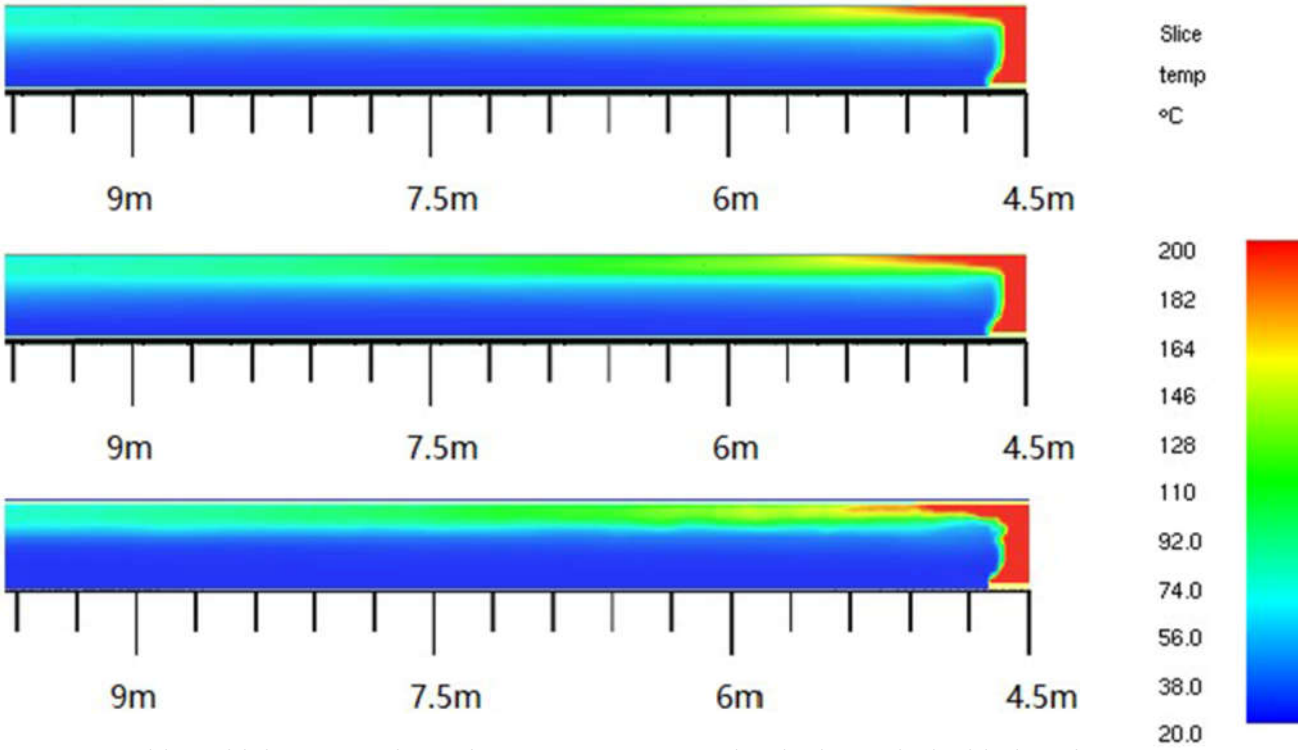

Figure5. Grid sensitivity: comparison of temperature contour plots in the vertical mid-plane for 3 mesh cell sizes for simulation 1 (Table 1): 2 cm × 2 cm × 2 cm (top), 1.5 cm × 1.5 cm × 1.5 cm (middle) and 1 cm × 1 cm × 1 cm (bottom).Values have been averaged over the period 100 s – 200s (steady heat release rate).

2.1.2 Water spray

In simulation 3, the water sprays are activated (Table 1).In FDS 6, numerical droplets are injected and subsequently treated in a Lagrangian way (McGrattan et al., 2013). The thermo-physical properties of water are applied. Still, a number of input parameters have to be determined. A sensitivity analysis is performed first to quantify the impact of those choices on the results and hence to make decisions on the values and options chosen.

- **Droplet size distribution**

In FDS 6, there are essentially three options to model the droplet size distribution: Rosin-Rammler (RR),log-normal (LN) and a combination (LN/RR). In the latter, the LN distribution is assumed for droplets with diameter smaller than the median volumetric diameter, $D_{v,50}$, while the RR distribution is applied for the larger droplets. The exact formulations for the distributions are found in (McGrattan et al., 2013).

The default option in FDS 6 is the combination 'LN/RR'. We compare results obtained with the default option to RR for Test 3 (i.e., in the absence of longitudinal ventilation). We use $D_{v,50} = 368\mu m$ and $\Upsilon = 3.5$ (Sun et al., 2016), because that value was reported in (Sun et al., 2016). It could be argued, though, that $D_{v,50} = 390\mu m$ and $\Upsilon = 3.0$ provides better agreement with the experimental data (Fig. 6). Therefore, the impact hereof is studied. The parameter $\sigma = 1.15/\gamma$ ensures a smooth connection at $D = D_{v,50}$ in the LN/RR distribution.

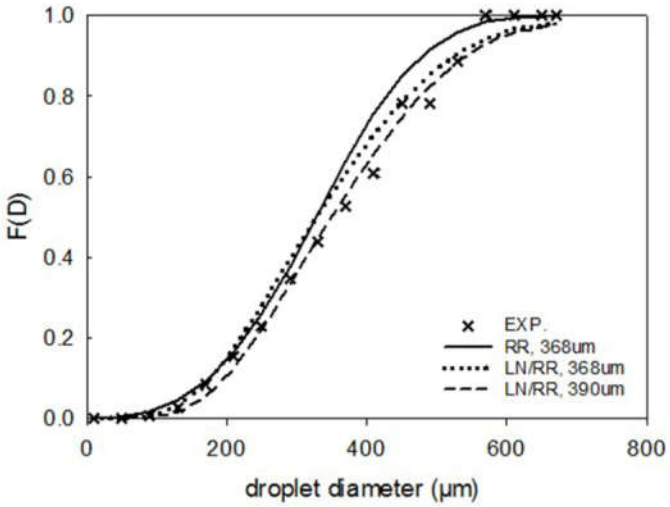

Figure6. Cumulative Distribution Function of droplet size distributions RR (Rosin-Rammler) and LN/RR (Lognormal- Rosin-Rammler), compared to experimental data (McGrattan et al., 2013).

Table 3 shows average temperatures at different positions. Values have been averaged over the steady state period(100s – 200s). The effect of the droplet size distribution on the temperatures is negligible. Also the effect on the flow field is very small (not shown). Therefore, the default LN/RR distribution is applied below.

Position	5-1	5-2	6-1	6-2	7-1	7-2	8-1	8-2	9-1	10-1	11-1
RR($D_{v,50}$=368um)	131.6	33.3	88.5	34.1	72.1	36.3	56.3	41.7	23.3	21.2	20.9
LN/RR($D_{v,50}$=368um)	132.4	33.4	88.4	34.0	72.0	35.9	56.3	41.1	23.2	21.3	20.9
LN/RR($D_{v,50}$=390um)	131.1	33.3	88.0	34.1	71.8	35.4	56.9	41.0	23.3	21.3	20.9

Table 3. Impact of the droplet size distribution on the temperatures for Simulation 3. Values have been averaged over the steady state period (100s – 200s).

- **Number of particles per second**

As mentioned, the actual water droplets are replaced by numerical particles, because it is impossible to track the high number of real water droplets. The number of particles injected into the computational domain per second, has to be specified by the user. The default value in FDS 6 is 5000(Sun et al., 2016). The lower this number, the shorter the computational time becomes. However, choosing this number too low can cause numerical instability(Sun et al., 2016).

In our sensitivity analysis, we used 3 values:5000(default), 10000 and100000. Table 4 illustrates some small impact with the very high number of particles per second on the temperatures (values have been averaged over the steady state period(100s – 200s)). Nevertheless, the significant increase in computational time (39 h with 5000, 42 h with 10000 and 72 h with 100000 particles per second) does not justify this choice. Therefore, we use the default value (5000 particles per second) in the simulations below.

Position	5-1	5-2	6-1	6-2	7-1	7-2	8-1	8-2	9-1	10-1	11-1
5000	131.6	33.3	88.5	34.1	72.1	36.3	56.3	41.7	23.3	21.2	20.9
10000	132.1	33.0	88.4	33.5	71.9	35.8	56.1	39.2	23.3	21.2	20.8
100000	129.7	33.8	86.9	33.6	71.1	35.5	54.3	38.7	23.4	21.1	20.7

Table 4. Impact of the number of particles injected per second on the temperatures for Simulation 3. Values have been averaged over the steady state period(100s – 200s).

- **Age**

The age of droplets indicates the number of seconds the particles remain in the computational domain. Once their 'age' is expired, the particles are removed from the calculation. Three different values are tested: 1s, 5s and 20s.The higher the value, the longer the computation times become (because more droplets are tracked in the steady state situation). Yet, it makes no sense to keep tracking droplets that reached the floor. For droplets of 100μm diameter, it takes about 1s to reach the floor (in the absence of ventilation), so for the large majority of droplets it takes less than 1 s. Table 5 confirms some very small deviation in the temperatures (values have been averaged over the steady state period(100s - 200s)) if the age is set to only 1s, and no difference is observed between the 5s and 20s age results. Therefore, we use the value 5s in the simulations below.

Position	5-1	5-2	6-1	6-2	7-1	7-2	8-1	8-2	9-1	10-1	11-1
1	132.1	33.8	87.9	34.7	71.6	37.1	55.1	40.6	23.6	21.5	21.1
5	130.6	32.0	87.5	31.7	71.9	33.0	56.4	40.7	23.1	20.7	20.4
20	130.9	31.4	88.0	30.9	71.7	33.1	57.5	39.8	23.0	20.5	20.1

Table 5. Impact of the parameter 'age' (in s) on the temperatures for Simulation 3. Values have been averaged over the steady state period (100s – 200s).

3 Simulation results

Figure 7 shows the temperature field in the vertical mid-plane (x = 0.56 m). Values have been averaged over the steady state period(100s – 200s).The impact of the water sprays is very clear

: the smoke layer (indicated by the increase in temperature) seems to be effectively blocked in this plane.

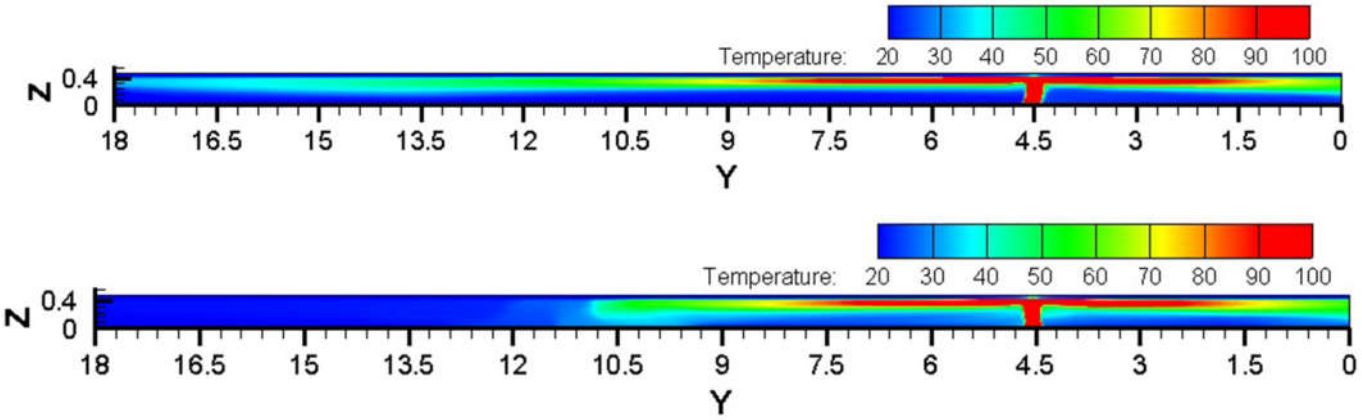

Figure 7. Temperature fields and velocity vectors in the vertical mid-plane (x=0.56m) for Test 1 (top) and Test 3 (bottom). Values have been averaged over the steady state period(100s – 200s).

The main purpose of this paper is, as mentioned, a more detailed analysis of the effect of the water sprays on the flow and temperature fields. Therefore, we focus on that region. Figure 8 provides a closer look in that region, including the vertical (w) and longitudinal (v) ventilation components. Values have been averaged over the steady state period(100s – 200s). It is recalled that the mid-plane (x = 0.56m) does not cross the nozzle heads (see below). The top figure (mean temperature) confirms the blocking of the smoke, i.e., temperature reduce significantly as soon as the hot smoke layer (flowing underneath the ceiling from the right to the left in the pictures) reaches the first sprays. Nevertheless, temperatures do remain clearly above ambient within the first spray envelope: smoke is entrained into the spray (see also below). The bottom figure, showing the longitudinal velocity component, clearly illustrates that, at the right hand side of the first sprays, the flow is diverted from horizontal (from right to left) underneath the ceiling to vertically downward (drag and blocking effect by the water spray) to horizontal (from left to right) at the floor (due to impingement of the water spray and the smoke onto the floor).

Before continuing the discussion of the flow field in the vertical mid-plane, it is instructive to first examine the temperature and flow field in the vertical plane that crosses 2 nozzle heads (x = 0.26m), Figure 9. The blocking effect, with at the same time entrainment of smoke into the first (i.e., the spray at the right), is clear, as was the case in Fig. 8. The bottom figure now also makes the entrainment of smoke into the sprays very clear (alternating

red and blue colors near the ceiling, illustrating alternating flow from the right to the left and vice versa). Also the impingement onto the floor is very clear in the bottom figure.

Interestingly, there is a clear upward motion in the region in between the sprays (middle figure of Fig. 9). This is caused by the two impinging jet flows in between the sprays, bumping onto each other and causing an upward flow as such. Going back to Figure 8 now, the impingement near the floor is less pronounced than it is observed in Fig. 9, but it is still clearly visible. The situation at the ceiling, though, is different from the situation in Fig. 9: in the vertical mid-plane, there is clear impingement of the upward flow in between the sprays towards the ceiling, rather than entrainment into the sprays. Indeed, the zone of upward motion (Fig. 8, middle figure), caused by the impinging flow regions bumping onto each other near the floor in the region in between the sprays, is much more pronounced in the vertical mid-plane than in the plane through the nozzle heads.

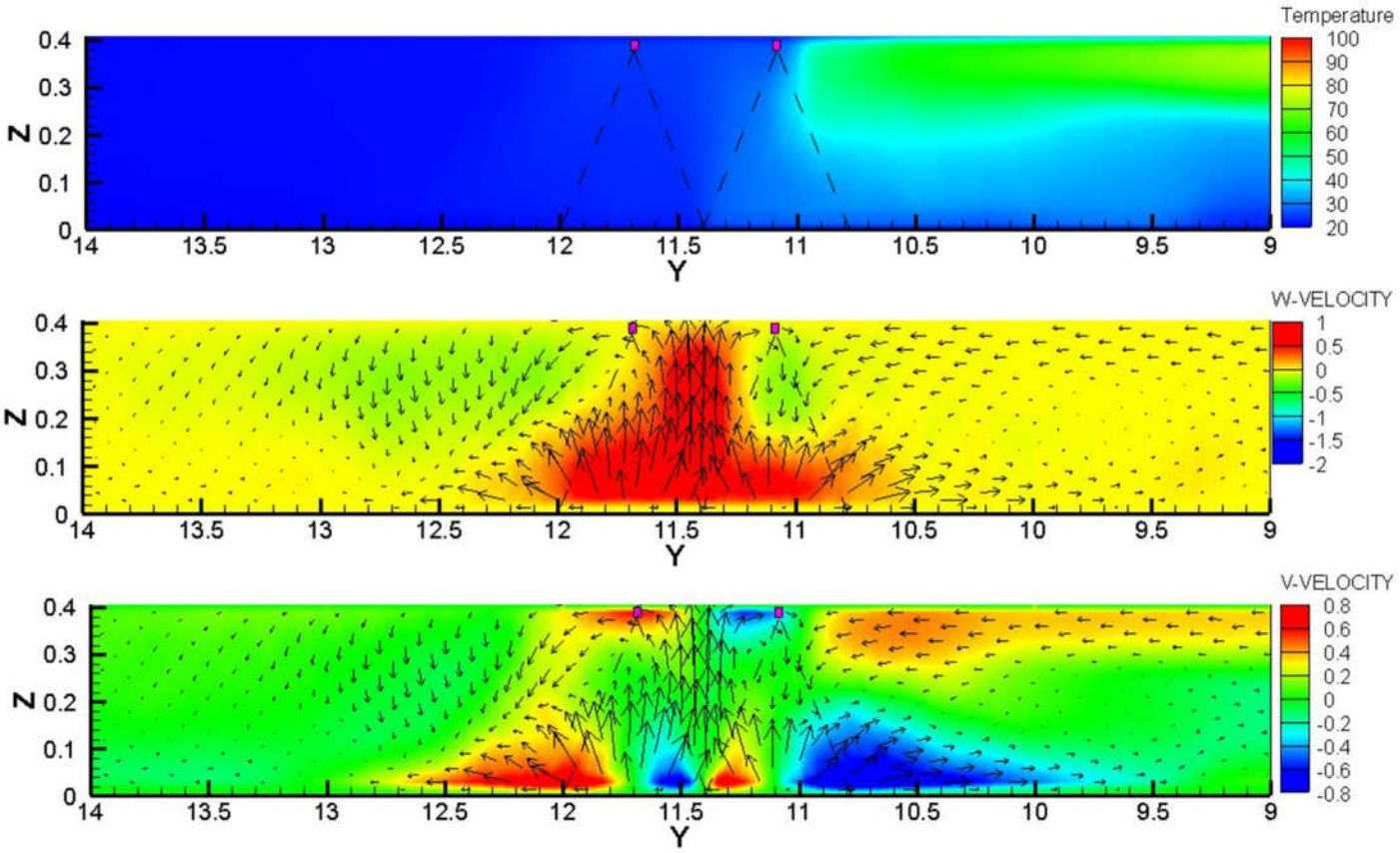

Figure 8. Temperature field (top), vertical velocity component (middle), longitudinal velocity component (bottom) and velocity vectors in the vertical mid-plane (x=0.56m) for Simulation 3. Values have been averaged over the steady state period(100s – 200s). The dashed lines indicate the spray envelopes (simplified representation as straight lines).

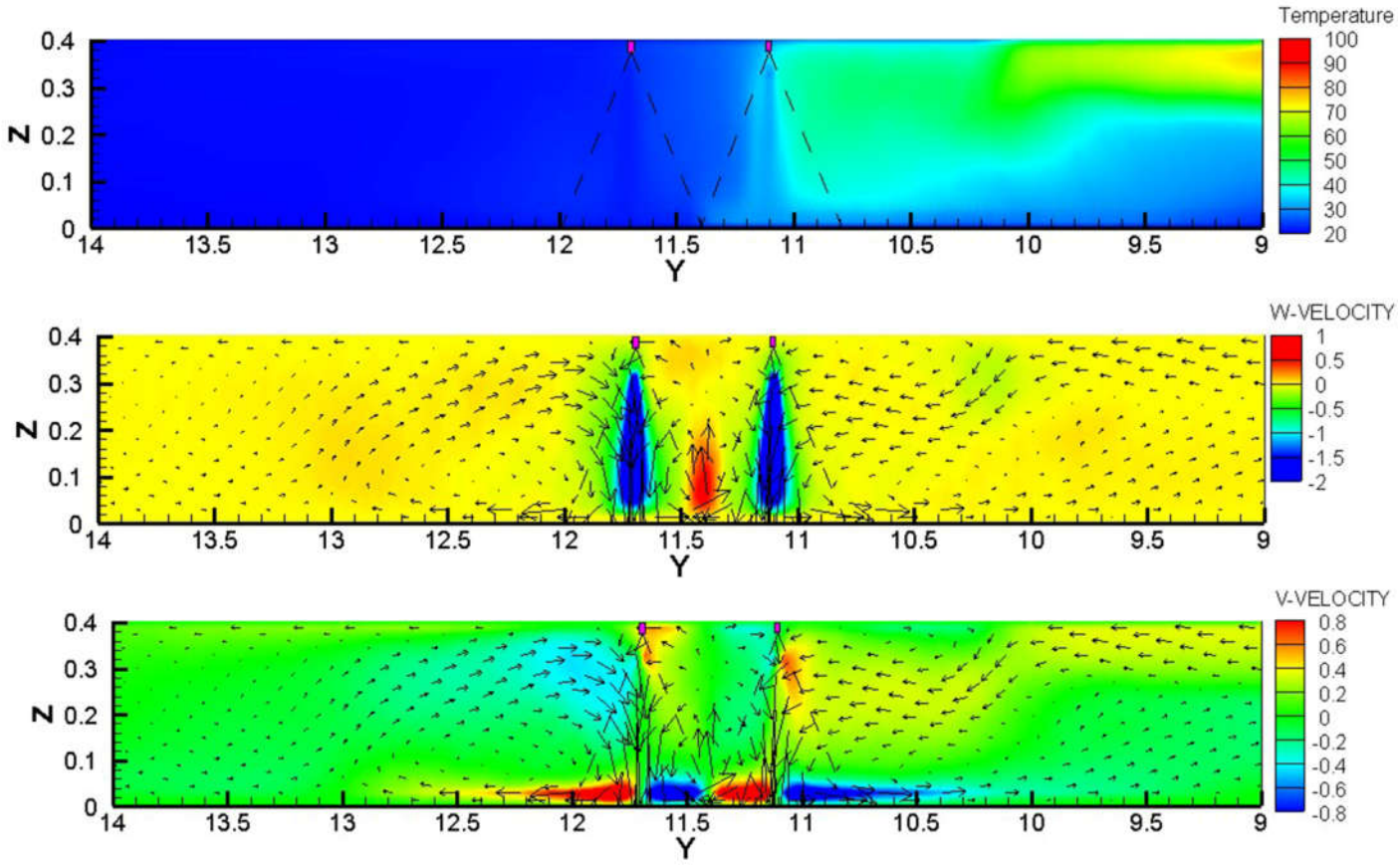

Figure 9. Temperature field (top), vertical velocity component (middle), longitudinal velocity component (bottom) and velocity vectors in the vertical plane through 2 nozzle heads(x=0.26m) for Simulation 3. Values have been averaged over the steady state period(100s – 200s). The dashed lines indicate the spray envelopes (simplified representation as straight lines).

The discussion on mean flow and temperature fields is completed by contour plots in horizontal planes at the positions of the thermocouples (z = 0.36m and z = 0.2m). Figure 10 shows the results at mid-height (z = 0.2m). Careful examination of the temperature contour plot reveals a slight temperature increase at the left hand side of the sprays, but this is small. Clearly the smoke can penetrate the most close to the walls. This is logical, because there is less coverage there by the sprays (in the central part, the sprays 'collaborate'). The middle figure clearly illustrates the upward motion in between the sprays. The bottom figure essentially shows the pattern related to the entrainment of air and smoke into the sprays (see Fig. 9: the plane z = 0.2 m, is in the entrainment zone). The

tendency for more flow to the left in the vertical mid-plane at z = 0.2m in the region of the sprays is due to the 'pushing' effect of the smoke (flowing from the right to the left).

Figure 11 shows the results near the ceiling (z = 0.36m). Again a small temperature increase is observed at the left hand side of the sprays. The most interesting observation, though, is the complex flow pattern, best illustrated by the longitudinal velocity component (bottom figure): there is a clear combination of entrainment into the sprays and impingement due to the upward flow in between the sprays. The pattern is not symmetric, due to the pushing effect of the smoke from the right to the left. This effect is more pronounced than in Fig. 10, because the smoke has more horizontal momentum near the ceiling: the horizontal flow has not yet been deflected into a vertically downward flow. It is noteworthy that the impingement effect of the upward flow in between the sprays assists in blocking the smoke.

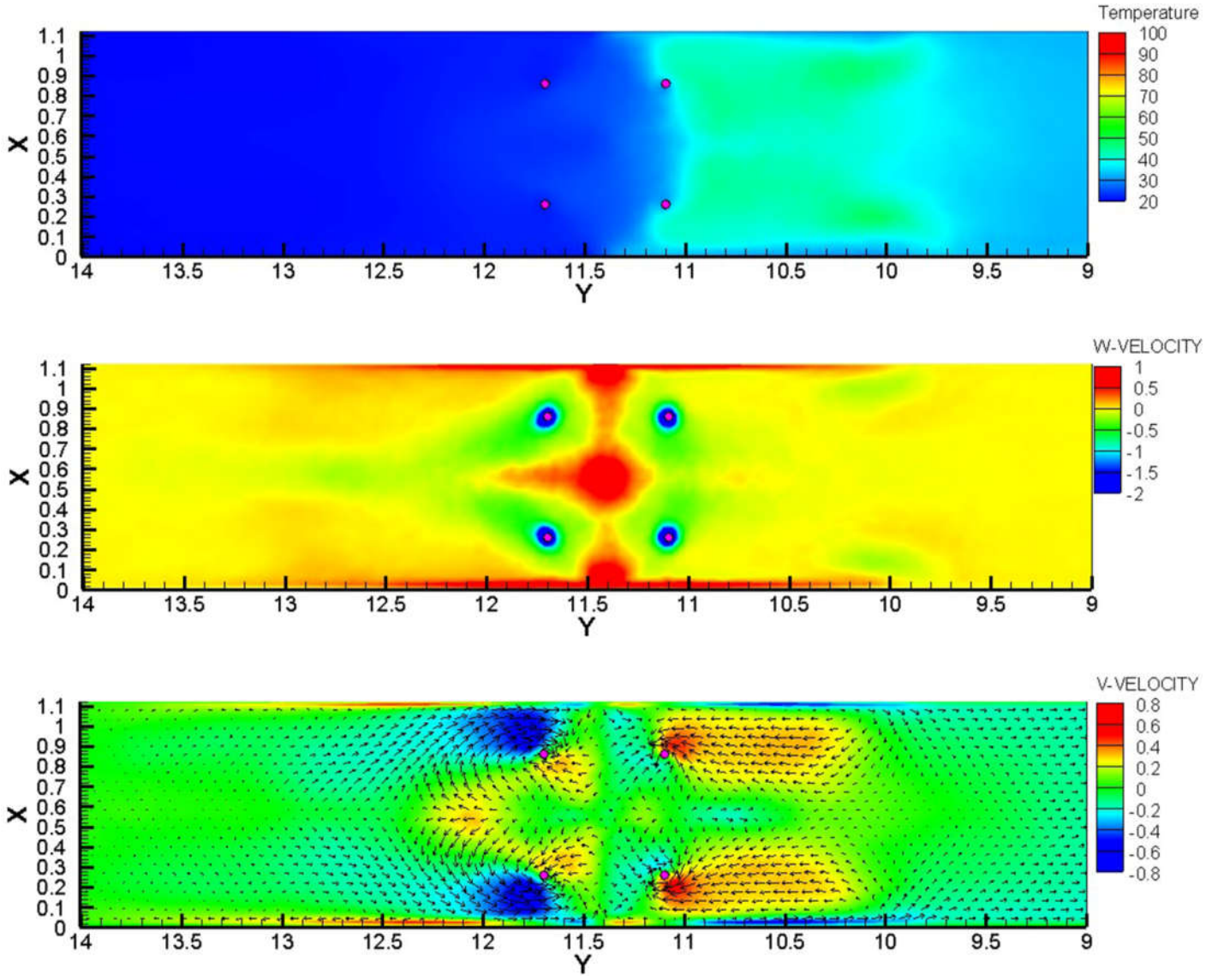

Figure 10. Temperature field (top), vertical velocity component (middle), longitudinal velocity component (bottom) and velocity vectors in the horizontal plane at mid-height(z =0.2m) for Simulation 3. Values have been averaged over the steady state period(100s – 200s).

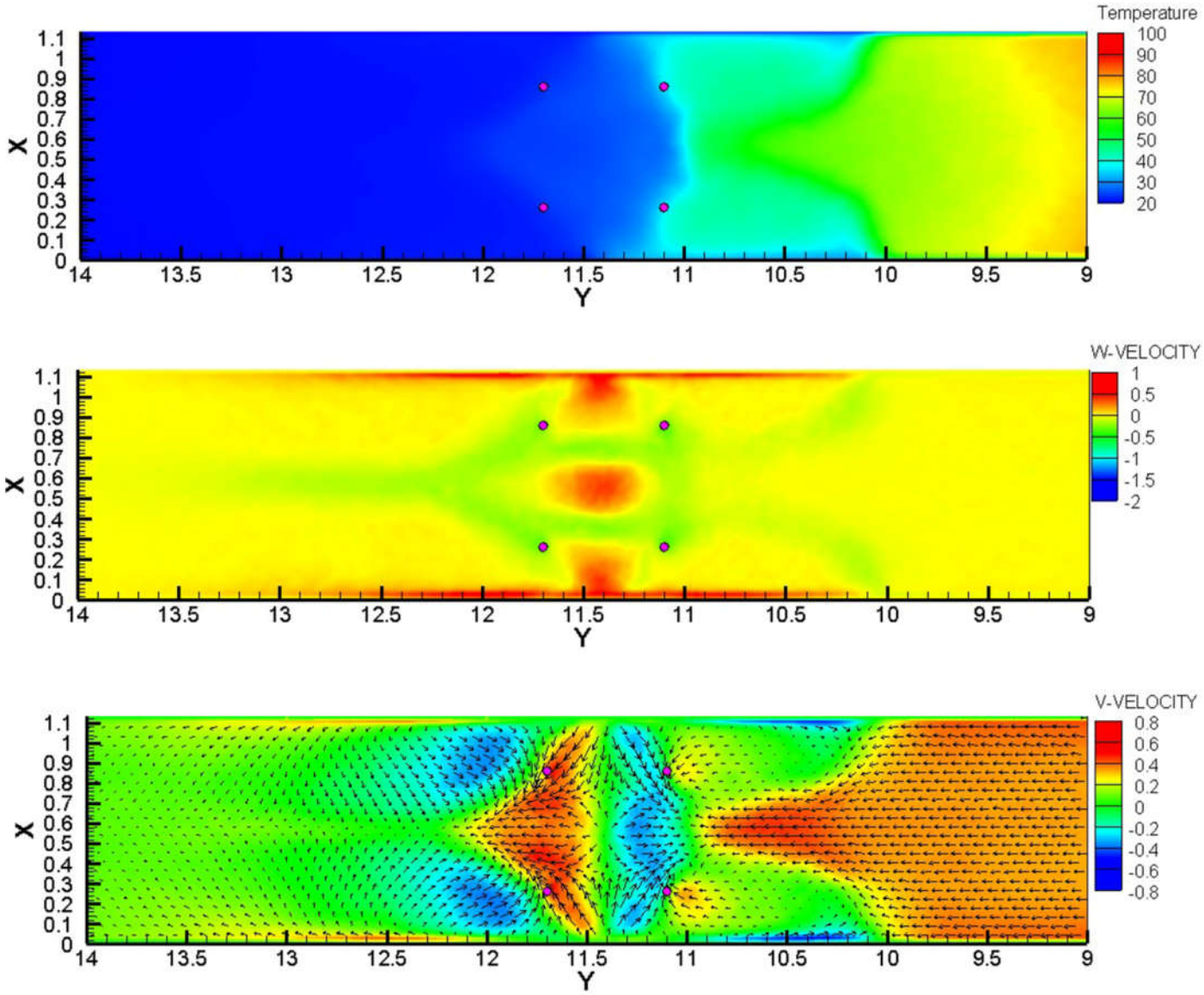

Figure 11. Temperature field (top), vertical velocity component (middle), longitudinal velocity component (bottom) and velocity vectors in the horizontal plane near the ceiling(z =0.36m) for Simulation 3. Values have been averaged over the steady state period(100s – 200s).

Obviously, it is important to verify the validity of the simulation results. Unfortunately, only temperature measurements are available. Figure 12 illustrates the agreement of the results obtained here with the experimental data at 3 positions for Tests 1 and 3: position 5 is close to the fire, position 7 is in between the fire and the sprays and position 10 is downstream of the sprays (see Table 2). The CFD results are considered very satisfactory, in

the sense that the global observation is well captured: results at points 5 and 7 essentially remain unaffected by the water spray, while there is a drastic reduction in temperature at point 10 upon activation of the water sprays. The over-prediction at position 5-1 during the early stages for test 1 is due to the variability in heat release rate evolution in the tests, as indicated in Fig. 2. In the simulations, always the same heat release rate evolution is imposed (Fig. 2). Similarly, this explains the temperature decay observed in the experimental data for Test 3 at position 5-1 from t = 160 s onwards: the peak heat release rate is obtained faster in Test 3 than in Test 1, so that the fuel burns out more rapidly. Fuel burn out has not been included in the simulations (Fig. 2), so obviously this decay is not captured. Most importantly, though, the absolute values agree very well in the steady state period, which is the most important phase for the study at hand, which focuses on the flow field during this period. There is some tendency towards over-prediction by FDS, but this may partly be due to smoke leakage (which was, as mentioned above, observed in the experiments, but not measured; leakage has not been accounted for in the simulations).

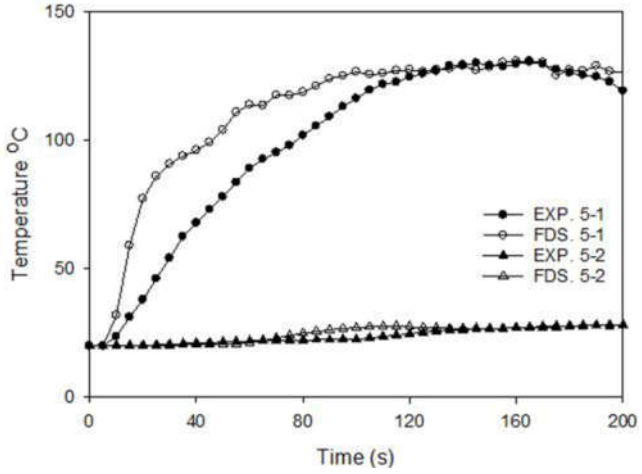
Temperature °C
Time (s)
EXP. 5-1
FDS. 5-1
EXP. 5-2
FDS. 5-2

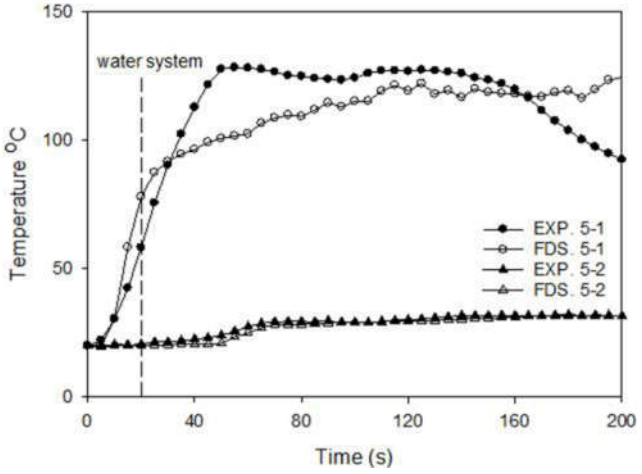
water system
Temperature °C
Time (s)
EXP. 5-1
FDS. 5-1
EXP. 5-2
FDS. 5-2

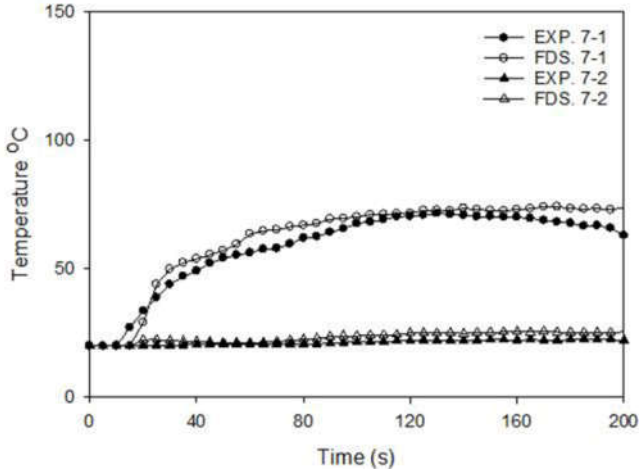
Temperature °C
Time (s)
EXP. 7-1
FDS. 7-1
EXP. 7-2
FDS. 7-2

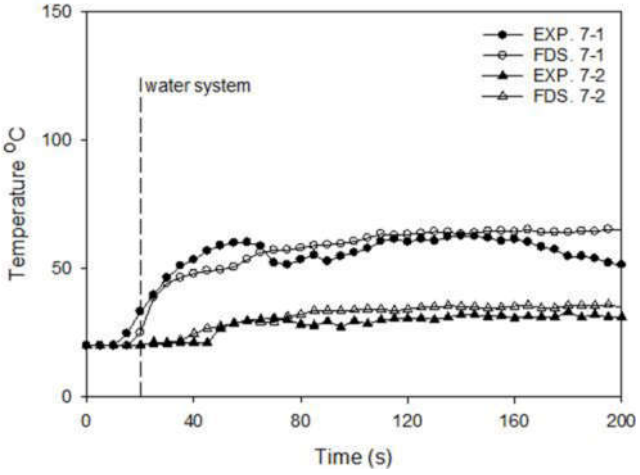
water system
Temperature °C
Time (s)
EXP. 7-1
FDS. 7-1
EXP. 7-2
FDS. 7-2

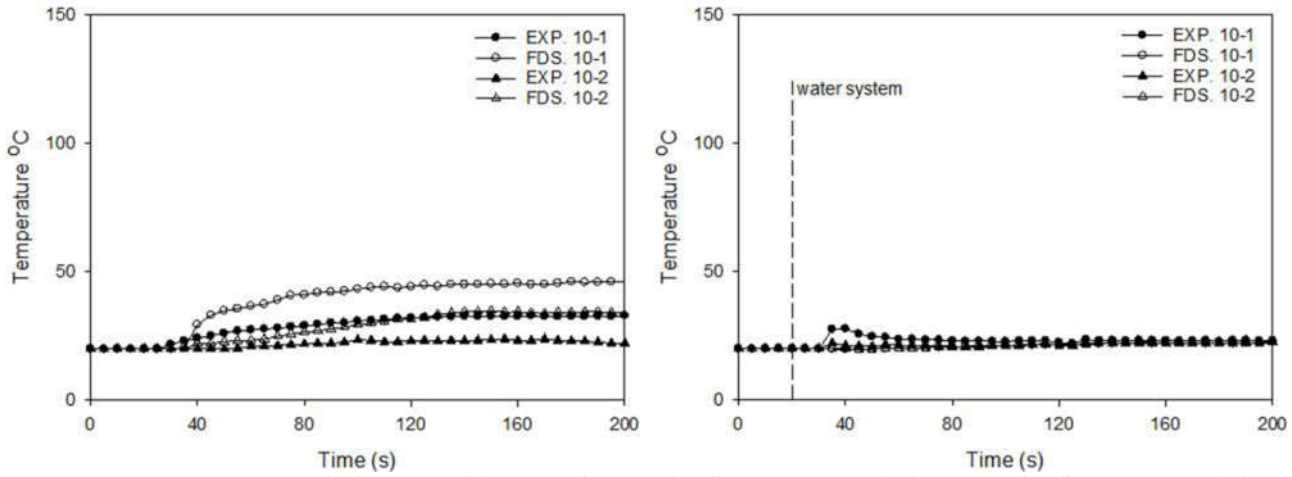

Figure12. Temperature evolution at positions 5 (close to the fire source), 7 (in between the fire source and the water sprays) and 10 (downstream of the water sprays) for Simulations 1 (left) and 3 (right).

4 Conclusions

The work described herein presents a set of CFD simulations, obtained with FDS, version 6.0.1 (McGrattan et al., 2013), of reduced-scale tunnel fire experiments (Sun et al., 2016).

First of all, a comprehensive sensitivity study has been presented on the computational mesh (for the flow) and model settings for the sprays. Default settings have been applied for turbulence, combustion and radiation. Temperature measurements have been used to illustrate the validity of the CFD simulations and the mesh sensitivity study allowed to decide on the mesh, so that the CFD results can be trusted as reliable.

Subsequently, the numerical study allowed to analyze in more detail the mechanisms leading to the smoke blocking effect of a water spray pattern induced by a set of 4 nozzles. More particularly, a close look at the flow field, which would be very difficult to obtain experimentally, revealed the presence of a clear upward motion in the region in between the sprays. Such motion is caused by spray-induced impinging jets onto the floor. These jets, induced by entrainment into the sprays, merge and create a zone of upward motion that acts as a ‘barrier’, preventing smoke spread downstream the water sprays. This blocking effect is particularly efficient in the absence of longitudinal ventilation.

5 Acknowledgements

This work was supported by National Natural Science Funds of China [grant numbers.51576144, 51508426] and China Scholarship Council [grant numbers 201306270111].

Tarek Beji is a Postdoctoral Fellow of the Fund for Scientific Research-Flanders (Belgium).

6 References

Blanchard, E., Boulet, P., Fromy, P., Desanghere, S., Carlotti, P., Vantelon, J., Garo, J., 2014. Experimental and numerical study of the interaction between water mist and fire in an intermediate test tunnel. Fire Technology 50, 565-587.

Chow, W., Yao, B., 2001. Numerical modeling for interaction of a water spray with smoke layer. Numerical Heat Transfer: Part A: Applications 39, 267-283.

Cooper, L.Y., 1995. The interaction of an isolated sprinkler spray and a two-layer compartment fire environment. Phenomena and model simulations. Fire Safety Journal 25, 89-107.

Deckers, X., Haga, S., Tilley, N., Merci, B., 2013. Smoke control in case of fire in a large car park: CFD simulations of full-scale configurations. Fire Safety Journal 57, 22-34.

Drysdale, D., 2011. An introduction to fire dynamics. John Wiley & Sons.

Hua, J., Kumar, K., Khoo, B.C., Xue, H., 2002. A numerical study of the interaction of water spray with a fire plume. Fire Safety Journal 37, 631-657.

Kim, S.C., Ryou, H.S., 2003. An experimental and numerical study on fire suppression using a water mist in an enclosure. Building and Environment 38, 1309-1316.

Li, Y., Chow, W., 2008. Study of water droplet behavior in hot air layer in fire extinguishment. Fire technology 44, 351-381.

McGrattan, K., Hostikka, S., McDermott, R., Floyd, J., Weinschenk, C., Overholt, K., 2013. Fire dynamics simulator, user's guide. NIST special publication 1019, 6thEdition.

McGrattan, K.B., Baum, H.R., Rehm, R.G., 1998. Large eddy simulations of smoke movement. Fire Safety Journal 30, 161-178.

Merci, B., 2014. Computer modeling for fire and smoke dynamics in enclosures: a help or a burden? Fire Safety Science 11, 46-65.

Merci, B., Van Maele, K., 2008. Numerical simulations of full-scale enclosure fires in a small compartment with natural roof ventilation. Fire safety journal 43, 495-511.

Morgan, H.P., Baines, K., 1979. Heat transfer from a buoyant smoke layer beneath a ceiling to a sprinkler spray. 2—an experiment. Fire and Materials 3, 34-38.

Sirignano, W.A., 1999. Fluid dynamics and transport of droplets and sprays. Cambridge university press.

St-georges, M., Buchlin, J.M., 1994. Detailed single spray experimental measurements and one-dimensional modelling. International Journal of Multiphase Flow 20, 979-992.

Sun, J., Fang, Z., Tang, Z., Beji, T., Merci, B., 2016. Experimental study of the effectiveness of a water system in blocking fire-induced smoke and heat in reduced-scale tunnel tests. Tunnelling and Underground Space Technology 56, 34-44.

Tang, Z., Fang, Z., Merci, B., 2014. Development of an analytical model to quantify downward smoke displacement caused by a water spray for zone model simulations. Fire Safety Journal 63, 89-100.

Tang, Z., Vierendeels, J., Fang, Z., Merci, B., 2013. Description and application of an analytical model to quantify downward smoke displacement caused by a water spray. Fire Safety Journal 55, 50-60.

Tilley, N., Rauwoens, P., Merci, B., 2011. Verification of the accuracy of CFD simulations in small-scale tunnel and atrium fire configurations. Fire Safety Journal 46, 186-193.

Van Maele, K., Merci, B., 2008. Application of RANS and LES field simulations to predict the critical ventilation velocity in longitudinally ventilated horizontal tunnels. Fire Safety Journal 43, 598-609.